

Full Waveform Inversion of the Scattered Component of the Wavefield: Resolution Analysis

Kirill Gadylshin(✉) and Maxim Protasov

Institute of Petroleum Geology and Geophysics, SB RAS, Novosibirsk, Russia
GadylshinKG@ipgg.sbras.ru

Abstract. The paper considers the influence of the scattered component of the wavefield on the full waveform inversion results. Utilizing the one step of the quasi-Newton method, we demonstrate that scattered wavefields bring helpful information in the context of the solution of the inverse dynamical problem. Theoretically, usage of the scattered waves should increase the resolution of the method. For different scenarios, the contribution of scattered waves is investigated numerically. We investigate the influence of scattered components only by using singular value decomposition of the linearized inverse problem operator. The numerical experiments are performed for the well-known Marmousi2 model.

Keywords: Scattering · FWI · SVD · Hessian pseudo-inversion

1 Introduction

The solution to an inverse dynamic seismic problem, the purpose of which is to restore the parameters of a geological section from a complete set of recorded seismograms, has long attracted the attention of researchers. In the mid-1980s, a practical approach to solving the inverse dynamic problem was proposed [1, 2]. The inverse problem was posed as the problem of minimizing the target functional characterizing (in a particular norm) the discrepancies of seismograms recorded in the field and synthetic ones, i.e., calculated seismograms. Synthetic seismograms are computed using some algorithm for modeling waveforms within the framework of the selected mathematical model, which describes the physical processes of seismic wave propagation in the medium with varying degrees of certainty. The appearance of the first works on this topic caused great enthusiasm among seismic prospectors. The term "Full Waveform Inversion" (FWI) was firmly entrenched in the professional community, which in the mathematical sense implies the solution of the inverse dynamic seismic problem.

FWI is a procedure for constructing high-resolution deep velocity models [3]. It is based on fitting the modeled seismic data with the raw field data by introducing a misfit functional with the subsequent application of local optimization

Supported by RSF grant 21-71-20002.

© The Author(s), under exclusive license to Springer Nature Switzerland AG 2022
O. Gervasi et al. (Eds.): ICCSA 2022, LNCS 13375, pp. 143–157, 2022.
https://doi.org/10.1007/978-3-031-10522-7_11

techniques. The algorithm starts with the best guess of the subsurface Earth model, which is then enhanced using the iterations of linearized local inversion for solving a nonlinear problem [4].

Experiments on real seismic data have shown that FWI does not achieve satisfactory results without setting an excellent initial medium model. It was shown that the initial model should correctly describe the behavior of the low-frequency (in space) components of the characteristics of the geological section, the so-called macro velocity model of the medium, which represents the propagation times of waves. Thus, a paradox arose since the macro model is of the most significant interest for constructing deep seismological sections, and it was the most challenging part of the inverse problem. The first reason was the absence in the recorded data of low frequencies (<7–10 Hz), which are most sensitive to disturbances of the macro model. This limitation was caused by the technical characteristics of the seismic data acquisition equipment that existed at that time. Currently, the acquisition tools allow to quite confidently register the low-frequency component of useful signals starting 3 Hz. The second reason, which is a consequence of the first, is the low sensitivity of the high-frequency components of the spectrum of the reflected wavefield to smooth variations in the velocity model of the medium. It was shown in [5,6] that the use of refracted waves makes it possible to significantly increase the sensitivity of the misfit functional to the macro velocity model and thereby fill in the missing information about the low-frequency component.

With standard seismic data processing, the obtained depth-velocity model focuses on the qualitative result of the migration of reflected waves. At the same time, the image result of scattered waves in such a model is not sufficiently focused. Therefore, to improve the quality of diffraction images, it is necessary to refine the migration model for which FWI is supposed to be used.

Theoretically [7], the resolution of the method when using scattered waves should be higher. In recent work [8], using a simple model example, it was shown that diffracted waves increase the resolution of the method. However, the influence of the scattered component of the wavefield on the inversion result has been poorly studied. In this work, we aim to assess the influence of the scattered component of the full waveform on the quality of the inverse dynamic problem solution.

2 Method

We assume that the wave process under study is described by the scalar Helmholtz Eq. (1) for a two-dimensionally inhomogeneous medium. Let $c(x, z)$ be the wave propagation speed in a two-dimensional medium. In what follows, it will be convenient to use the value $m = c^{-2}(x, z)$ (the squared slowness) for the solution of the inverse problem. We will call m a model and write $m \in M$, meaning by M some space of models. Let the function $u(x, z; \omega)$ (full waveform in the time-frequency domain) satisfy the Helmholtz equation:

$$(\Delta + \omega^2 m)u = -f, \tag{1}$$

with the right-hand side $f(x, z)$ and angular frequency ω. The principle of limiting absorption determines the behavior at infinity of this solution:

$$\begin{aligned} u &= \lim_{s \to +0} u_s; \\ (\Delta + (\omega + i\epsilon)^2 m) u_s &= -g; \\ u_s \to 0, &\quad \sqrt{x^2 + z^2} \to \infty. \end{aligned} \tag{2}$$

By operator of the forward problem $\mathcal{F}_f(m; \omega)$ we mean a mapping that assigns a function $m(x, z)$ to a solution of Eq. (1). When the right-hand side of this equation has the form $g(x, z; \omega) = f(\omega)\delta(x - x_s)\delta(z - z_s)$, the corresponding operator will be denoted by $\mathcal{F}_{x_s}(m; \omega)$. One should note that the result of the action of this operator coincides with the product of the spectral characteristic of source signature $f(\omega)$ and the Green's function $G(x, x_s, z, z_s; m; \omega)$. The waveform in the time-frequency domain is a complex function of the position of the point (x, z) and the frequency ω. The inverse problem is to determine the velocity model of the medium from the wavefield recorded at a finite number of points in R^2 where the geophones are located. Let us introduce a linear operator that calculated the trace of the full wavefield from one point source for a fixed time frequency at the points corresponding to the location of the receivers:

$$P : U \to C^{NR}, \tag{3}$$

where NR is the number of receivers. If all NS sources with coordinates (x_i, z_i) are used, then the data space for each of them at a fixed frequency ω_j is determined by the action of the following operator, which transfers an element m from the model space to a vector from the space C^{NR}:

$$F_i^j(m) = P \cdot \mathcal{F}_{x_i}(m; \omega_j). \tag{4}$$

In what follows, we will also use a compact notation:

$$F(m) = \begin{pmatrix} F^1(m) \\ \vdots \\ F^{NF}(m) \end{pmatrix}, \tag{5}$$

where $F^j : M \to C^{NS \times NR}$ such that:

$$F^j(m) = \begin{pmatrix} F_1^j(m) \\ \vdots \\ F_{NS}^1(m) \end{pmatrix}. \tag{6}$$

Finally, we obtain the following forward modeling operator:

$$F : M \to D, \tag{7}$$

where the data space $D = C^{Nf \times NS \times NR}$. In this notation, the inverse dynamical problem of constructing a velocity model from seismic data is reduced to solving a nonlinear operator equation:

$$d^{obs} = F(m_{true}), \tag{8}$$

here d^{obs} – is the observed data and m_{true} – the "true" velocity model. The Full Waveform Inversion (FWI) applies a nonlinear least-squares method to Eq. (8). The general FWI formulation is to find the minimum point of the misfit functional characterizing the mean square deviation of the recorder data from those calculated for the current velocity model:

$$m_* = arg(\min_{m \in M} ||F(m) - d||_D^2). \tag{9}$$

3 Numerical Experiments

3.1 Marmousi2 Synthetic Model

We carry out all considerations using the synthetic velocity model shown in Fig. 1: a modified Marmousi2 P-wave velocity model [9]. We perform the seismic full waveform modeling using the finite-difference solver in the time-frequency domain for Eq. (1) for the following source-receiver acquisition geometry: 320 volumetric point sources were at line $z = 0$ m starting at $x = 500$ m with equal step 50 m. We use the geometry of the receiver (one measures the pressure) with a regular step of 25 m, and the maximum source-receiver offset equals 6000 m. For forward modeling, we exclude all effects associated with the presence of multiple waves caused by a free surface in the medium by introducing the absorbing layers around the numerical domain [10].

3.2 Diffraction FWI Resolution Analysis

Let us introduce the following notation:

- m^* – is the Marmousi2 model after addition the depth point diffractors (Fig. 2 A);
- m_0 – is the starting model for the inversion (Fig. 2 B);
- $dm1$ – is the desired velocity perturbation we wish to recover using FWI (Fig. 2 C);
- dm_{diff} – are depth point diffractors (Fig. 2 D).

In this notation, the full model m^* is represented as follows:

$$m^* = m_0 + dm1 + dm_{diff}. \tag{10}$$

Consider the original statement of the inverse dynamic seismic problem $d^{obs} = F(m_{true})$. Using the notation introduced above, we have:

$$\begin{aligned} d^{obs} = F(m^*) = F(m_0 + dm1 + dm_{diff}) = \\ F(m_0 + dm_{diff}) + \frac{\delta F}{\delta m}(m_0 + dm_{diff})dm1 + \\ o(\|dm1\|_M) = \\ F(m_0) + \frac{\delta F}{\delta m}(m_0)dm_{diff} + \frac{\delta F}{\delta m}(m_0 + dm_{diff})dm1 + \\ o(\|dm1\|_M) + o(\|dm_{diff}\|_M). \end{aligned}$$

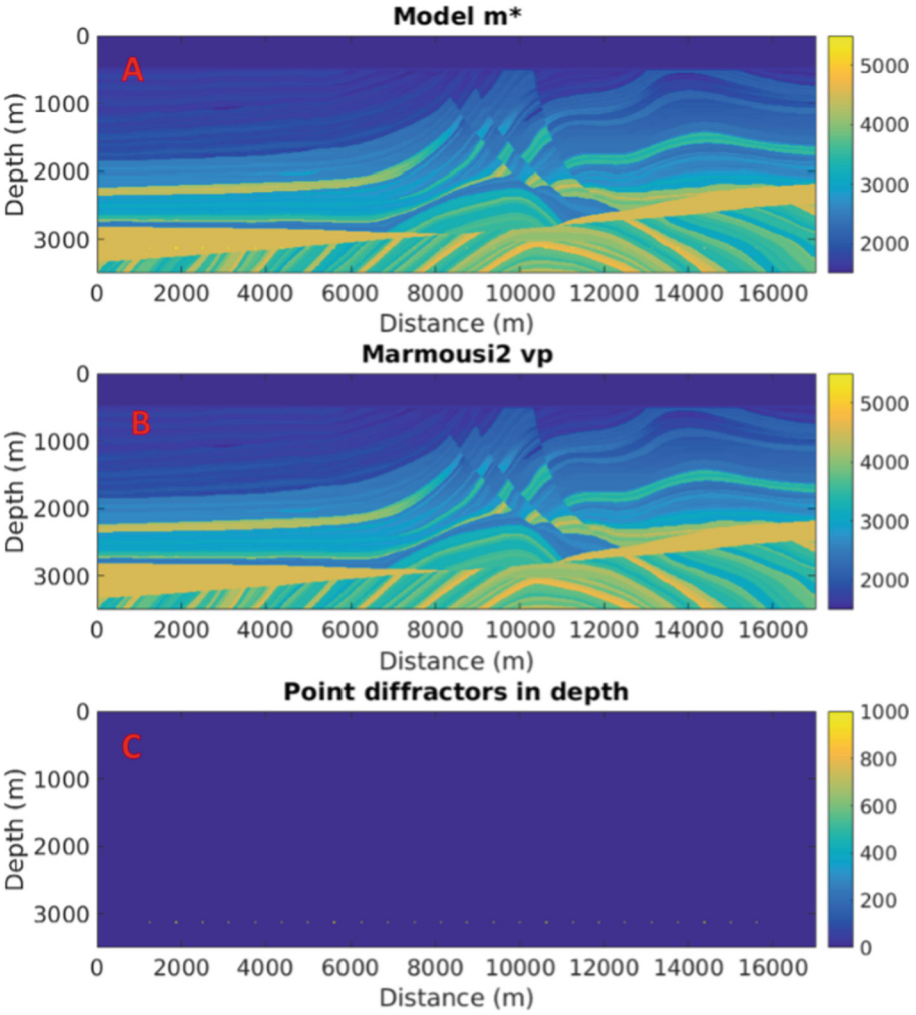

Fig. 1. The model Marmousi2 with point diffractors at 3100 m (A), the original Marmousi2 model (B), and the difference between (A) and (B).

The last expression can be rewritten as:

$$\frac{\delta F}{\delta m}(m_0 + dm_{diff})dm1 \approx d^{obs} - F(m_0) - \frac{\delta F}{\delta m}(m_0)dm_{diff}. \tag{11}$$

Based on this expression, there is a clear connection between the model perturbation and the corresponding perturbation in the data. The scattered component of the wavefield associated with the presence of deep point diffractors (3100 m) is a very small order of magnitude (the norm $\|dm_{diff}\|_M$ is an order of magnitude smaller than the norm of the desired perturbation $\|dm1\|_M$). This explains such behavior of the FWI procedure in the standard formulation. The

strongest events in terms of amplitude are described first, which entails significant updates to the velocity model. How can this be bypassed? We see the two options:

1. In the first option all considerations are carried out for the starting model m_0. It is proposed in formula (11) to neglect intense events on the right side (the difference $d^{obs} - F(m_0)$), and try to make a linearized inversion: $\frac{\delta F}{\delta m}(m_0 + dm_{diff})dm1 = -\frac{\delta F}{\delta m}(m_0)dm_{diff}$ The latter can be expressed via regularized solution (r-Solution, see [12]):

$$dm1_r = -\Big(\frac{\delta F}{\delta m}(m_0 + dm_{diff})\Big)^{-1}_r \frac{\delta F}{\delta m}(m_0)dm_{diff}. \tag{12}$$

2. The second option inspires more confidence in success. It is based on considering an approximate calculation of the Hessian, its pseudo-inversion, followed by the action on the gradient, built only on the diffraction component (for more details, see below).

Option 1. To construct an r-pseudoinverse operator, it suffices to calculate only the highest singular vectors corresponding to the highest singular numbers. The inverse operator is not considered in the entire space of models but only in the subspace of lower dimension spanned by the highest r right singular vectors of the original linear operator (in our case, this operator is $\frac{\delta F}{\delta m}(m_0 + dm_{diff})$).

The choice of the parameter r depends on the behavior of the singular spectrum and the condition number of the corresponding truncated system of linear equations obtained after performing a finite-difference approximation of the integral equation of the first kind (see [14]). An iterative Arnoldi method was used to speed up numerical calculations to construct the highest singular numbers and the corresponding singular vectors, which does not require an explicit specification of the matrix [15]. Its implementation was performed using the specialized library SLEPc (Scalable Library for Eigenvalue Problem Computations), oriented towards high-performance computing systems with parallel architecture (see: http://www.grycap.upv.es/slepc/). To carry out calculations, one needs to set the parameter r, i.e., the dimension of stable space, and have a subroutine that calculates the action of a matrix on an arbitrary vector. Such a subroutine was created based on a finite-difference solution of the Helmholtz equation. In this case, an LU-decomposition of the matrix is constructed for each frequency from a given range. The matrix is determined by a finite-dimensional approximation of the Helmholtz operator. After obtaining the LU-factors for all frequencies, the iterative finding of eigenvectors is reduced to a specific set of forward and backward substitutions. Now let us return to the parameters of the numerical experiment. Since the calculation of singular value decomposition (SVD) is a very resource-intensive task, and on most computing clusters, the calculation time is limited to 24 h, it is necessary to choose the calculation parameters carefully. By running a series of test runs (trial and error), we settled on the following parameters:

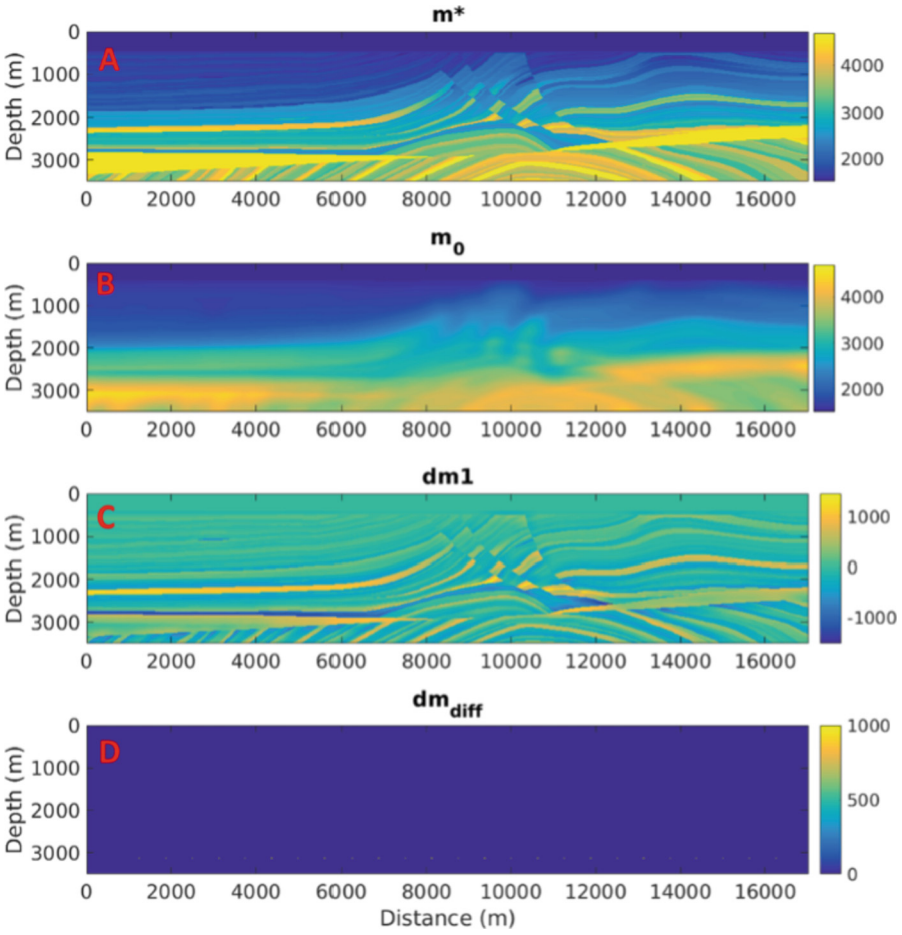

Fig. 2. Velocity model m^* (A), starting model (B), the desired velocity perturbation (C), and depth point diffractors (D).

- calculation grid with steps $dx = dz = 15$ m;
- the target area has a size of 147×400 pixels (see Fig. 3);
- the step by sources had to be thinned and made equal to 100 m (total 160 sources of the expansion point type);
- the number of frequencies for an inversion - 4: {5, 7, 10, 14} Hz (what causes this choice, we will describe below).

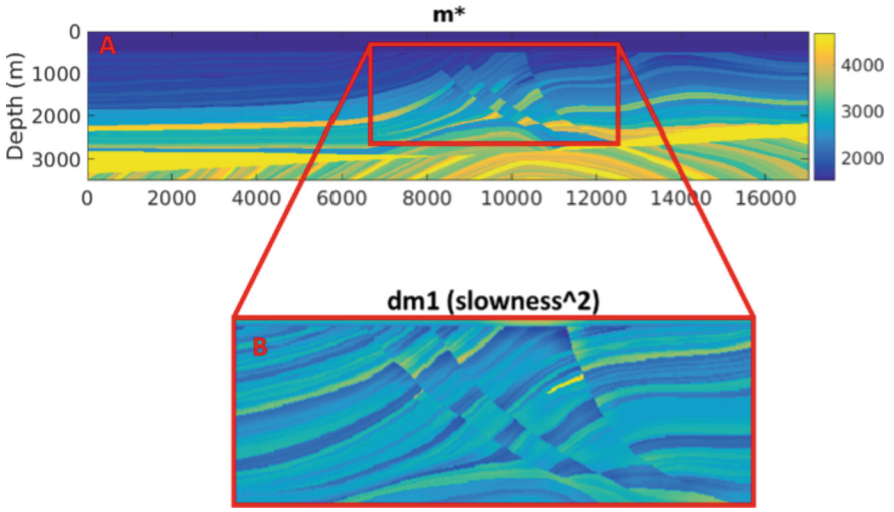

Fig. 3. Velocity model m^* (A). The unknown perturbation $dm1$ (B) is plotted on a scale corresponding to the square of slowness. The target area for inversion and SVD analysis is depicted in red. (Color figure online)

As noted above, when choosing the optimal parameters, our goal is to compromise the resolution of the problem and the computation time. The lower and upper timing frequencies 5 Hz and 14 Hz, respectively. The choice of the lower one is due to strict requirements for the quality of input data – in practice, it is rarely possible to find informative frequencies 5 Hz, even if we are talking about marine data. Since we plan to investigate the influence of the scattered component of the full wavefield on the inversion results for the so-called middle or transitional temporal frequencies, we choose the upper frequency equal 14 Hz. Low temporal frequencies, in this terminology, are frequencies up 2 Hz, which are necessary for the stable reconstruction of a smooth model or a model that is kinematically equivalent to the true one. Our starting model is good enough not to need the lower time frequencies in this experiment. High frequencies are the frequencies responsible mainly for the reflected component of the wavefield. The choice of the target area is because this part of the model is complex and is of the greatest interest for inversion (Fig. 3). It is also worth noting that we get a complete observation system with this choice of the target area (there are no edge effects associated with poor illumination).

A source step of 100 m is sufficient for the inversion, at least for a qualitative assessment of the result. By choosing a step of 100 m instead of 50 m, forward and backward substitutions are sped up by about two times. As a result, the entire SVD calculation time is sped up by two times. Let us describe in more detail the choice of time frequencies for inversion. On the one hand, each temporal frequency is considered independently and in parallel, and the calculation of the action of the matrix on the vector should not change significantly. The more

time frequencies we consider, the slower the singular spectrum of the operator decreases (the same one can say about the number of sources, the fewer there are, the faster the spectrum decreases, but this dependence is not linear). The optimal set of frequencies will be carried out following the work [16]. For our observation system, the maximum offset is 6000 m, while the depth of the target area is less than 3000 m. Therefore $\alpha_{min} = \frac{1}{\sqrt{2}}$, $f_0 = 5$ Hz, $f_1 = \frac{f_0}{\alpha_{min}} \approx 7$ Hz, $f_2 = \frac{f_1}{\alpha_{min}} \approx 10$ Hz, and $f_3 = \frac{f_2}{\alpha_{min}} \approx 14$ Hz. It is argued that this choice of temporal frequencies provides continuous coverage of spatial frequencies in the reconstructed model during FWI in the range [5, 14] Hz for a given observation system.

Singular spectra (first 768 values) for operators $\frac{\delta F}{\delta m}(m_0 + dm_{diff})$ and $\frac{\delta F}{\delta m}(m_0)$ are presented in Fig. 4.

As one may observe, they are almost indistinguishable. If we take the ratio of these values (Fig. 4 C), we can see that this value is nearly equal to 1. From this, we can conclude that these operators are almost indistinguishable from solving the inverse problem. In confirmation of this, we present several random comparisons of the right singular vectors of these operators corresponding to the same singular numbers. Such a comparison is shown in Fig. 5.

Option 2. Consider the objective function of the standard FWI method:

$$E(m) = \|F(m) - d^{obs}\|_D^2. \tag{13}$$

Assume that we have the operator for extracting the scattered component of the wavefield:

$$P_{diff} : D \to D, \tag{14}$$

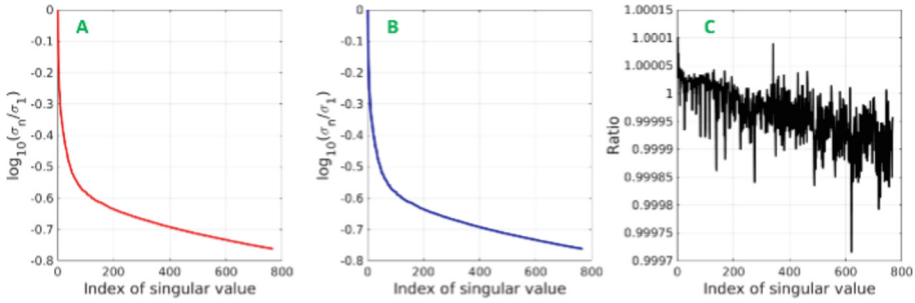

Fig. 4. Singular spectrum of $\frac{\delta F}{\delta m}(m_0)$ operator (A), $\frac{\delta F}{\delta m}(m_0 + dm_{diff})$ operator (B), and their ratio (C).

for simplicity, we assume that this operator is linear and self-adjoint. Then the changed formulation of the FWI oriented on the use of the scattered component have the following objective function:

$$\widetilde{E}(m) = \|P_{diff}F(m) - P_{diff}d^{obs}\|_D^2. \tag{15}$$

Then the modified objective functional gradient $\nabla\widetilde{E}(m)$ will take the form:

$$\nabla\widetilde{E}(m) = -Re\Big(\frac{\delta F}{\delta m}^*(m)P_{diff}^*\Delta d\Big), \tag{16}$$

where $\Delta d = P_{diff}F(m) - P_{diff}d^{obs}$. Under our assumption that P_{diff} is linear and self-adjoint, finally (16) will take the form:

$$\nabla\widetilde{E}(m) = -Re\Big(\frac{\delta F}{\delta m}^*(m)(P_{diff}F(m) - P_{diff}d^{obs})\Big). \tag{17}$$

We have carried out two numerical experiments. In each experiment, we assumed that the correct velocity model was obtained by adding a finite number of point diffractors (Figs. 6 C, 6 D) to the model shown in Fig. 6 A. Thus, the scattered component of the full waveform is the difference between the solutions of the wave equation calculated in the model with diffractors and in the model without them (see Fig. 7). In terms of solving the inverse problem, we can assume that at the first step of inversion, the residual $P_{diff}F(m) - P_{diff}d^{obs}$ is built without any explicit statement of the operator. Indeed, we have no point diffractors in the starting model, therefore $P_{diff}F(m_0) = 0$. $P_{diff}d^{obs}$ could be obtained as follows: $P_{diff}d^{obs} = F(m_0 + dm1 + dm_{diff}) - F(m_0 + dm1)$ since this difference is due only to the presence of the point diffractors. It is worth noting here that after the first inversion step, it will no longer be possible to extract the scattered component without explicitly constructing the operator P_{diff}. Therefore, we will concentrate on obtaining the maximum information in one step of the nonlinear least-squares method. To do this, we will resort to Newton's method, which states that the choice of the direction of updating the model should be such that the gradient calculated in the updated model is zero, we have reached the extreme value: $\nabla\widetilde{E}(m + dm) = 0$. The last brings us to the following expression:

$$H(m)dm = -\nabla\widetilde{E}(m), \tag{18}$$

where $H(m)$ is the Hessian of the objective functional (15). The Hessian approximation by neglecting terms that include the second derivative of the forward modeling operator [13] leads us to the following expression for updating the model:

$$dm_r = -\Big(\frac{\delta F}{\delta m}(m)\frac{\delta F}{\delta m}^*(m)\Big)_r^{-1}\nabla\widetilde{E}(m) \tag{19}$$

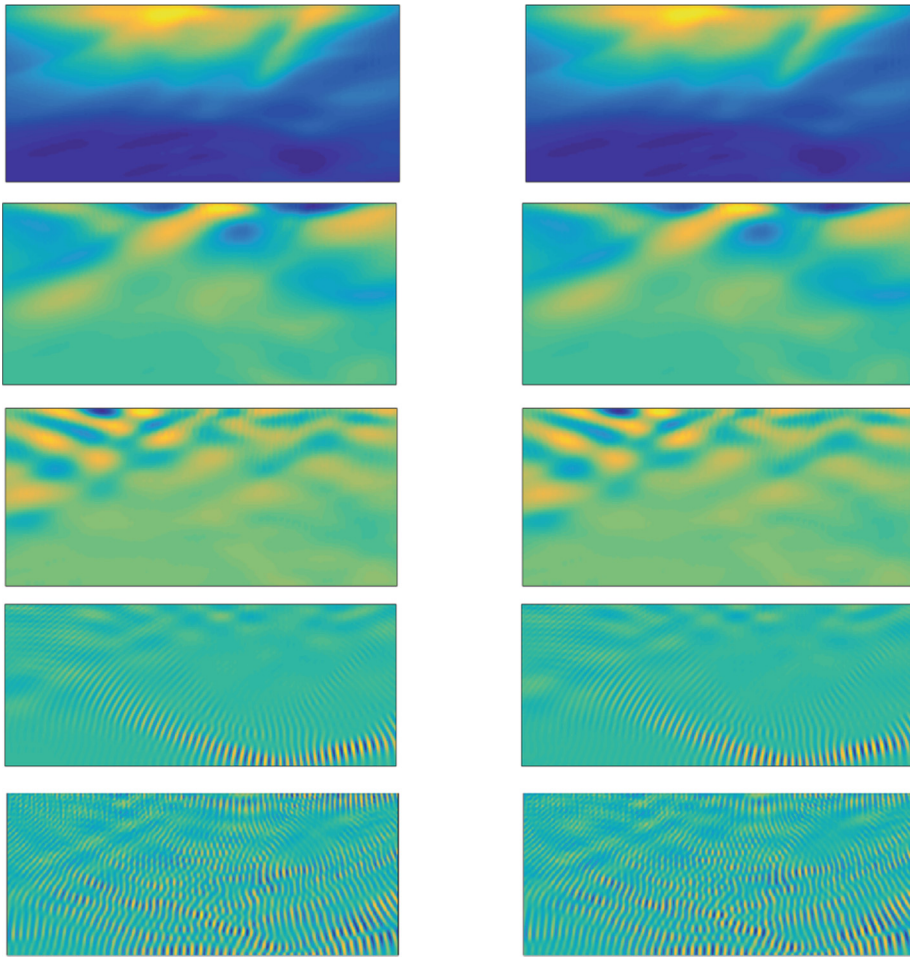

Fig. 5. The comparison of the right singular vectors of the operator $\frac{\delta F}{\delta m}(m_0 + dm_{diff})$ – left column, and $\frac{\delta F}{\delta m}(m_0)$ – right column. From top to bottom, different random indexes of the corresponding singular vectors.

here $-\left(\frac{\delta F}{\delta m}(m)\frac{\delta F}{\delta m}^*(m)\right)_r^{-1}$ r-pseudoinverse operator, whose action we will calculate through the singular value decomposition of the first Fréchet derivative $\frac{\delta F}{\delta m}(m)$ [14].

The solution to the inverse problem within the framework of the modified Newton method was constructed for a group of time frequencies [5, 7, 10, 14] Hz. The parametrization of the velocity model is the value equal to the square of the slowness. In the first experiment, the effect of only depth point diffractors was investigated (Fig. 6 C). In contrast, point scatterers were added to the entire model (except for the upper 500 m thick water layer). The models restored by

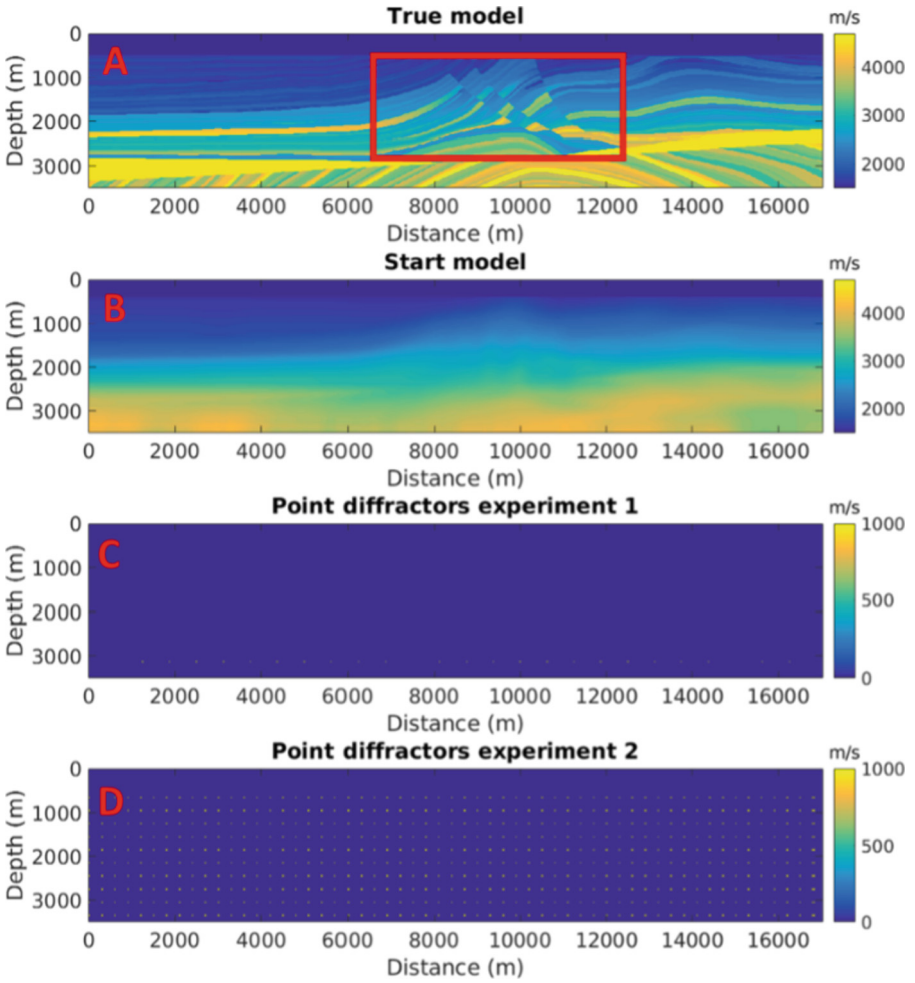

Fig. 6. The Marmousi2 velocity model (A), the starting model for performing the FWI (B), and two scenarios for point diffractors locations: depth point diffractors at the depth 3100 m (C) and uniformly spaced point diffractors throughout the velocity model (D). The target area for the inversion is shown as a red rectangle. (Color figure online)

formula (19) are shown in Fig. 8. As can be seen, even involving only the scattered component in the inversion process carries information about the structure of the medium. When one uses only depth point diffractors the result has a poor resolution. While using a larger number of scatterers increases the quality of the solution to the inverse problem.

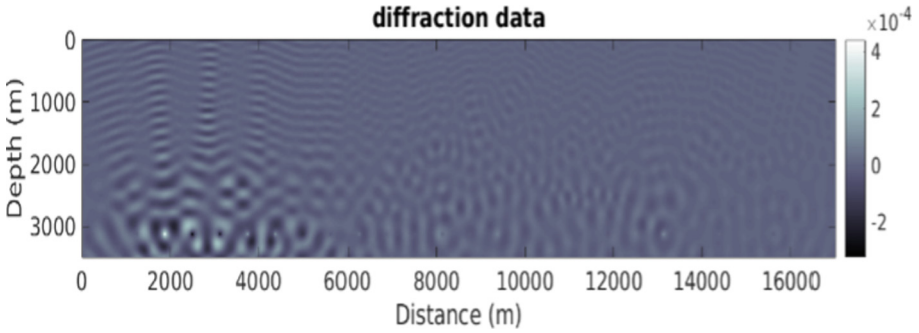

Fig. 7. Scattered component of the full wavefield for a frequency 10 Hz in the modified Marmousi2 model, associated with the presence of point diffractors located at a depth of 3100 m (see Fig. 5C). The source is located at the point x = 2800 m.

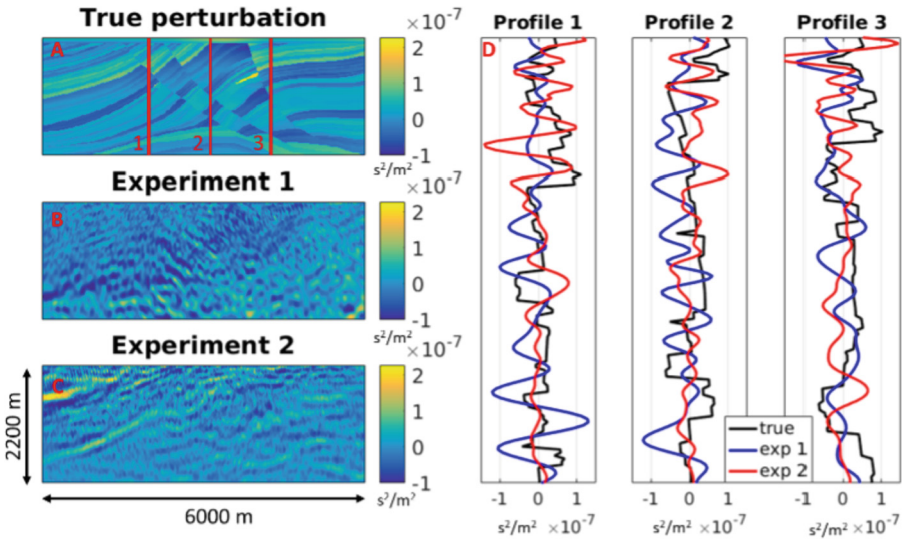

Fig. 8. Desired perturbation of the model (A), inversion results for Experiment 1 (B) and Experiment 2 (C). On the right (D), vertical profiles are shown corresponding to the positions marked with red lines on the graph on the left (A): black is the desired perturbation, blue and red are the reconstructed perturbations in experiments 1 and 2, respectively. (Color figure online)

4 Conclusions

The influence of the scattered component on the results of the FWI method has been studied. We enhance the inversion workflow by incorporating the r-pseudo-inverse approximate Hessian operator into the inversion process. We investigate one step of the nonlinear least-squares method. For two inversion scenarios, we demonstrate the contribution of scattered waves to the solution of the inverse

dynamic problem. For the case with deep point diffractors, the resolution of the method is low. When point scatterers are evenly distributed throughout the model, the resolution of the method increases. The last experiments show the possibility of improving the velocity model via full-waveform inversion of diffracted/scattered waves. Finally, we conclude one needs to construct an operator to extract the scattered component of the wavefield and enforce it inside the nonlinear inversion iteration process to provide an algorithm for the full-waveform inversion of diffracted/scattered waves.

Acknowledgements. The work is supported by RSF grant 21-71-20002. The numerical results of the work were obtained using computational resources of Peter the Great Saint-Petersburg Polytechnic University Supercomputing Center (scc.spbstu.ru).

References

1. Lailly, P.: The seismic inverse problem as a sequence of before stack migrations. In: Bednar, J.B., Robinson, E., Weglein, A. (eds.) Conference on Inverse Scattering-Theory and Application, pp. 206–220. SIAM, Philadelphia (1983)
2. Tarantola, A.: Inversion of seismic reflection data in the acoustic approximation. Geophysics **49**(8), 1140–1395 (1984). https://doi.org/10.1190/1.1441754
3. Virieux, J., Operto, S.: An overview of full-waveform inversion in exploration geophysics. Geophysics **78**, WCC1–WCC26 (2009). https://doi.org/10.1190/1.3238367
4. Warner, M., et al.: Anisotropic 3D full-waveform inversion. Geophysics **78**, R59–R80 (2013). https://doi.org/10.1190/geo2012-0338.1
5. Pratt, R.G., Song, Z.M., Williamson, P.R., Warner, M.: Two-dimensional velocity model from wide-angle seismic data by wavefield inversion. Geophys. J. Int. **124**(2), 323–340 (1996). https://doi.org/10.1111/j.1365-246X.1996.tb07023.x
6. Shipp, R.M., Singh, S.C.: Two-dimensional full wavefield inversion of wide-aperture marine seismic streamer data. Geophys. J. Int. **151**(2), 325–344 (2002). https://doi.org/10.1046/j.1365-246X.2002.01645.x
7. Khaidukov, V., Landa, E., Moser, T.J.: Diffraction imaging by focusing-defocusing: An outlook on seismic superresolution. Geophysics **69**(6), 1372–1570 (2004). https://doi.org/10.1190/1.1836821
8. Dell, S., Abakumov, I., Znak, P., Gajewski, D., Kashtan, B., Ponomarenko, A.: On the role of diffractions in velocity model building: a full-waveform inversion example. Stud. Geophys. Geod. **63**(4), 538–553 (2019). https://doi.org/10.1007/s11200-019-0733-6
9. Martin, G.S., Wiley, R., Marfurt, K.J.: Marmousi2: an elastic upgrade for Marmousi. Lead. Edge **25**(2), 156–166 (2006). https://doi.org/10.1190/1.2172306
10. Grote, M., Sim, I. : Efficient PML for the wave equation. Report arXiv:1001.0319 (2010). https://arxiv.org/abs/1001.0319
11. Protasov, M., Tcheverda, V.: True/preserving amplitude seismic imaging based on Gaussian beams application. In: SEG Technical Program Expanded Abstracts 2006, pp. 2126–2130 (2006). https://doi.org/10.1190/1.2369957
12. Cheverda, V.A., Kostin, V.I.: R-pseudoinverses for compact operators in Hilbert spaces: existence and stability. J. Inverse Ill-Posed Probl. **3**(2), 131–148 (1995). https://doi.org/10.1515/jiip.1995.3.2.131

13. Pratt, R.G., Shin, Ch., Hick, G.J.: Gauss-Newton and full Newton methods in frequency-space seismic waveform inversion. Geophys. J. Int. **133**(2), 341–362 (1998). https://doi.org/10.1046/j.1365-246X.1998.00498.x
14. Gadylshin, K., Bakulin, A., Dmitriev, M., Golikov, P., Neklyudov, D., Tcheverda, V.: Effect of free-surface related multiples on near surface velocity reconstruction with acoustic frequency domain. In: Proceedings 76th EAGE Conference and Exhibition 2014, LNCS, vol. 2014, pp. 1–5. European Association of Geoscientists & Engineers (2014). https://doi.org/10.3997/2214-4609.20141410
15. Hernandez, V., Roman, J.E., Tomas, A.: Parallel Arnoldi Eigensolvers with enhanced scalability via global communications rearrangement. Parallel Comput. **33**(7–8), 521–540 (2007). https://doi.org/10.1016/j.parco.2007.04.004
16. Sirgue, L., Pratt, R.G.: Efficient waveform inversion and imaging: a strategy for selecting temporal frequencies. Geophysics **69**(1), 231–248 (2004). https://doi.org/10.1190/1.1649391